DOI 10.5012/bkcs.2010.31.9.2503

# Growth and Characterization of Conducting ZnO Thin Films by Atomic Layer Deposition

**Yo-Sep Min,* Cheng Jin An, Seong Keun Kim,† Jaewon Song,† and Cheol Seong Hwang†**

*Department of Chemical Engineering, Konkuk University, Seoul 143-701 Korea. *E-mail: ysmin@konkuk.ac.kr*
*†WCU Hybrid Materials Program, Department of Materials Science and Engineering and Inter-university Semiconductor Research Center, Seoul National University, Seoul 151-744, Korea*
*Received March 16, 2010, Accepted July 13, 2010*

ZnO thin films were grown on Si or $SiO_2$/Si substrates, at growth temperatures ranging from 150 to 400 °C, by atomic layer deposition (ALD) using diethylzinc and water. Despite the large band gap of 3.3 eV, the ALD ZnO films show high *n*-type conductivity, i.e. low resistivity in the order of $10^{-3}$ Ωcm. In order to understand the high conductivity of ALD ZnO films, the films were characterized with X-ray diffraction, transmission electron microscopy, X-ray photoelectron spectroscopy, elastic recoil detection, Rutherford backscattering, Photoluminescence, and Raman spectroscopy. In addition, the various analytical data of the ZnO films were compared with those of ZnO single crystal. According to our analytical data, metallic zinc plays an important role for the high conductivity in ALD ZnO films. Therefore when the metallic zinc was additionally oxidized with ozone by a modified ALD sequence, the resistivity of ZnO films could be adjusted in a range of $3.8 \times 10^{-3} \sim 19.0$ Ωcm depending on the exposure time of ozone.

**Key Words**: ZnO, Conducting, Atomic layer deposition, Thin film

## Introduction

Zinc oxide (ZnO) is an *n*-type semiconductor with a wide band gap of 3.3 eV.[1-3] Recent progress in processing ZnO has opened up numerous applications for varistors, phosphors, sensors, UV light emitters, transparent high power electronics, surface acoustic wave devices, piezoelectric transducers, and optoelectronic devices.[4] Not only bulk crystal and thin films of ZnO but nano-structured ZnO such as nanowires and nanoparticles have been also intensively studied for various applications.[5]

ZnO thin films have been grown by various methods such as spray pyrolysis,[6] sol-gel,[7] sputtering,[8] chemical bath deposition,[9] metal-organic chemical vapor deposition,[10] and atomic layer deposition (ALD).[11-16] The ALD method is a special modification of chemical vapor deposition for self-limiting film growth.[17] The precursor vapor and reaction gas are alternately pulsed onto a substrate. The reaction chamber is purged with an inert gas between the pulses of precursor vapor and reaction gas. All the process steps are performed at low temperature, usually lower than 400 °C, to avoid thermal decomposition of the chemisorbed precursor molecules.

Assuming the hypothetical situation of a perfect pure single crystal without any defects, ZnO would be an insulator rather than a semiconductor at room temperature.[2] However, in the practically-obtained single crystal, the resistivity of ZnO is in the order of $10^2$ Ωcm.[18] Furthermore, ZnO thin films show a wide range of resistivity variation from ~$10^{-4}$ to ~ $10^8$ Ωcm, depending on the growth process condition.[1-3] Carcia *et al.* showed that the resistivity of ZnO films is increased from ~$10^{-2}$ to ~ $10^8$ Ωcm by increasing oxygen partial pressure in sputtering method.[8] Kohiki *et al.* also showed that the resistivity ($10^7$ Ω cm) of an as-grown ZnO film was dramatically decreased to $10^{-3}$ Ωcm for a film doped by hydrogen implantation.[19]

Because most ZnO is strongly *n*-type, it has been long assumed that the dominant donor is a native defect, either the oxygen vacancy ($V_O$), or the zinc interstitial ($Zn_I$).[20] However, the $V_O$ is no longer considered to contribute to the high conductivity because its energy level is too deep in the band gap of ZnO.[21-23] Recently, Van de Walle reported that the cause of the high conductivity of ZnO is hydrogen which incorporates in high concentrations and behaves as a shallow donor.[21] The role of hydrogen was also experimentally examined with sputtered ZnO:H films of which resistivity reached $2 \times 10^{-4}$ Ωcm.[24]

On the other hand ZnO films grown by ALD generally show high *n*-type conductivity with a low resistivity in the order of $10^{-2} \sim 10^{-3}$ Ωcm.[11,12] However, the high *n*-type conductivity of the ALD ZnO films is not clearly understood yet due to the complexity of its trasport behavior and lack of characterization for the ALD ZnO films. In this report, ZnO films were grown by ALD using diethylzinc (DEZ) and water as a Zn precursor and an oxidant, respectively. We investigated the growth behavior and electrical properties of ZnO films. The films were characterized to understand the high conductivity of ALD ZnO by various analytical methods such as X-ray diffraction (XRD), transmission electron microscopy (TEM), X-ray photoelectron spectroscopy (XPS), elastic recoil detection (ERD), Rutherford backscattering (RBS), Photoluminescence (PL), and Raman spectroscopy. In addition, the various analytical data of the ALD ZnO films were compared with those of a single crystalline ZnO. The effect of oxidant on the conductivity of ZnO films was also investigated by using ozone as an additional oxidant.

## Experimental Section

ZnO thin films were deposited on 8-inch bare silicon wafers for Figure 1 or $SiO_2$ (100 nm)/Si substrates for other figures, at deposition temperatures ranging from 150 to 400 °C, by using DEZ and water. The feeding time of water vapor was 2 s, and that of DEZ was varied from 0.1 to 3 s to confirm the self-

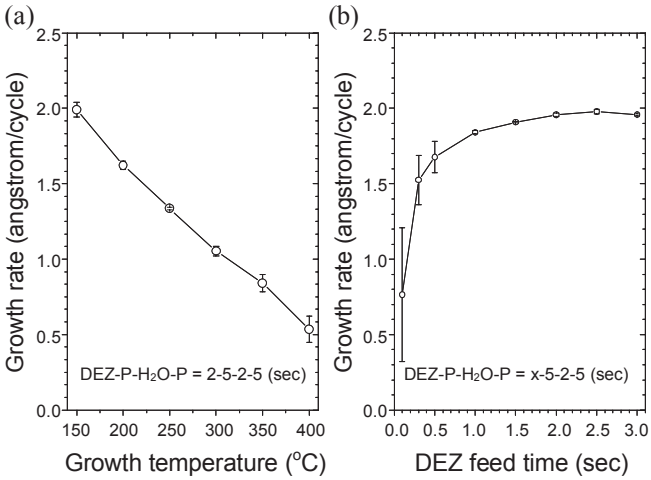


**Figure 1.** Growth behavior of ZnO films by ALD. (a) Growth rate as a function of growth temperature. (b) Growth rate at 150 °C as a function of DEZ feed time. The error bars denote standard deviations of the growth rates obtained from 9 different positions in an 8-inch substrate.

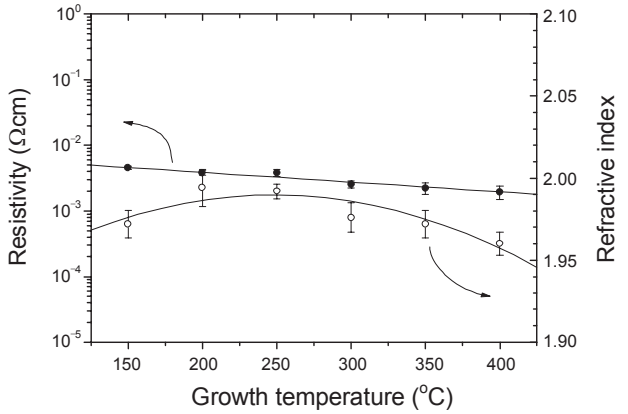


**Figure 2.** Resistivity (solid circles) and refractive index (open circles) of 50 nm-thick ZnO films on $SiO_2$ (100 nm)/Si substrates as a function of growth temperature. The error bars denote standard deviations of the values obtained from 9 different positions in an 8-inch substrate.

limiting growth behavior as shown in Figure 1b. The purging times were 5 seconds under Ar flow of 1600 sccm. DEZ and water were vaporized at room temperature, and delivered without any carrier gas to the reactor. The reactor pressure during the ALD process was around 0.6 Torr.

The film thickness and refractive index were determined by a spectroscopic ellipsometer (J. A. Woollam Co., Inc.) with a Cauchy dispersion model. The preferred orientation and crystal structure were examined by XRD measurements in θ/2θ scan mode with Cu Kα radiation and cross sectional high resolution TEM. For a comparison with the ALD ZnO films, an O-face polished ZnO single crystal (MTI Corp., 99.99%, <0001>) was used as a reference for XPS, PL and Raman spectroscopy. XPS measurements were performed on a Quantum 2000 Microprobe PHI spectrometer using a monochromatized Al Kα emission. Binding energies were measured using the C 1*s* peak (284.8 eV) of the adventitious carbon as an internal standard. Sputtering during the XPS depth profile was performed with 0.5 keV $Ar^+$ ions. The O/Zn ratio and hydrogen content in the films were analyzed by RBS and ERD, respectively. The optical properties of ZnO were characterized at room temperature by PL with a He-Cd laser as a light source using an excitation wavelength of 325 nm, and the laser powers were 6 mW/$cm^2$ for the films and 2 mW/$cm^2$ for the single crystal, respectively. Raman scattering measurements were performed in 180° backscattering geometry by using a 488 nm laser excitation. The carrier-type, concentration and mobility were measured using a Hall measurement with the Van der Pauw electrode configuration under a magnetic field of 0.5 T at room temperature.

## Results and Discussion

Figure 1 shows ZnO growth behavior by ALD. The growth rates in Figure 1a and 1b were determined from ZnO films grown on bare Si wafers for 300 and 100 cycles, respectively. The growth rate of ZnO films largely depends on the growth temperature, as shown in Figure 1a, which was also reported by others.[11,15] In this ALD reactor and process conditions, the growth rate linearly decreases from ~ 2 Å/cycle at 150 °C to 0.53 Å/cycle at 400 °C. From the growth rate uniformity over an 8-inch substrate, it was determined that the proper temperature window of ALD is in a range of 200 ~ 300 °C wherein the standard deviations in thicknesses are lower than 3%. The standard deviation of the film thickness grown at 400 °C is about 16%, possibly due to thermal decomposition of DEZ. Figure 1b shows the variation in growth rate as a function of feeding time for DEZ. The self-limiting growth behavior of ZnO thin films can be confirmed by this experiment. In the low feeding time of DEZ below 0.5 s, the standard deviations of the growth rate are large, but the sufficient supply of DEZ over 2 s gives small standard deviations with a saturated growth rate of ~ 2 Å/cycle at 150 °C.

For characterization of ZnO films, around 50 nm-thick ZnO films were grown on $SiO_2$ (100 nm)/Si substrates at different temperatures. The refractive index of a bulk ZnO at 589 nm is 2.00 ~ 2.02 but those of ZnO films are smaller than the literature value as shown in Figure 2 (open circles).[25] However, the refractive index increases as the growth temperature approaches the proper ALD region (200 ~ 300 °C).

Resistivity of the ALD ZnO films is in the order of $10^{-3}$ Ωcm showing a decreasing tendency at higher growth temperatures as shown in Figure 2 (solid circles). These values agree well with the reported values.[11,12] However it is much lower than ~ 380 Ωcm of ZnO single crystal grown by the hydrothermal method.[18]

Figure 3 shows Hall mobility and carrier concentration of ZnO films as a function of growth temperature. The mobility is 19 ~ 20 $cm^2$/Vsec in the temperature range of 150 ~ 250 °C and then rapidly decreases down to 8.1 $cm^2$/Vsec at 400 °C. However, the mobility values are much lower than that (~ 200 $cm^2$/Vsec) of single crystal.[18] The electron carrier concentration responsible for the *n*-type conductivity of ZnO films increases in the order of $10^{19}$ ~ $10^{20}$ /$cm^3$ as the growth temperature increases. Comparing the carrier concentration of the bulk crystal with the order of $10^{13}$ /$cm^3$,[18] the high electronic carrier con-

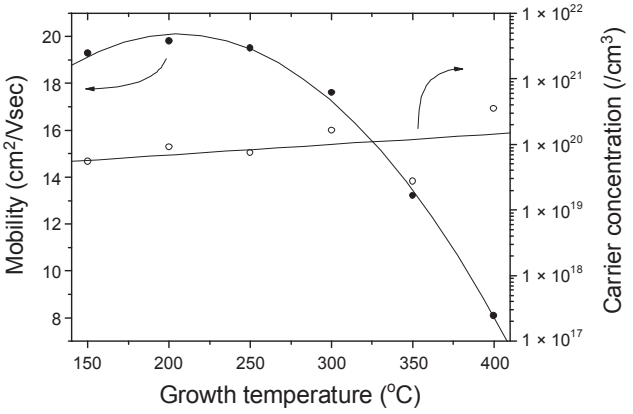


**Figure 3.** Electron mobility (solid circles) and carrier concentration (open circles) as a function of growth temperature.

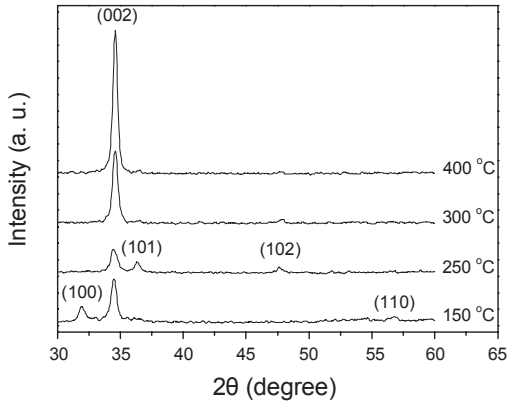


**Figure 4.** XRD patterns of the ZnO films grown at growth temperatures of 150, 250, 300 and 400 °C.

centration means that the donor-like defects such as $Zn_I$, $V_O$ and/or hydrogen were highly incorporated in the ZnO films. As growth temperature increases over 250 °C, the electron mobility decreases but the carrier concentration increases. The opposite tendency can be explained by the impurity scattering. Electron mobility generally decreases with increasing carrier concentration because the impurity scattering increases in proportional to its carrier concentration. However, the nearly-constant mobility in the growth temperature region of 150 ~ 250 °C reveals that there are other factors which contribute the electron mobility. Those may be grain size and crystallographic orientation of crystallites in the ZnO films as discussed in the following section.[26]

In the XRD patterns of Figure 4, the films grown at higher temperatures than 300 °C show a <002> preferred orientation, of which (002) planes are parallel to the substrate surface. However those grown at lower temperatures than 250 °C show a random orientation. Figure 5a and 5c show cross sectional TEM images of ZnO films grown at 250 and 400 °C, respectively. It is clearly observed that both films are grown with columnar grains, but the film grown at 400 °C has slightly larger grains than that grown at 250 °C. In scanning electron microscopic and atomic force microscopic images of the film surfaces (see the Supplementary Materials), the grain size is weakly dependent on the growth temperature and the root-mean-square (rms) roughness of the films was 0.5 ~ 1.1 nm. Figure 5b and 5d show high resolution TEM images of ZnO grown at 250 and 400 °C, respectively. The film grown at 400 °C is better crystallized with a more preferred growth orientation than that grown at 250 °C, as also revealed in the digital diffractogram.

Since the wurtzite structure of ZnO is anisotropic in the crystallographic aspect, ZnO shows anisotropic mobility due to piezoelectric scattering. The piezoelectric scattering acts only in the direction of the hexagonal *c* axis, thereby causing a reduc-

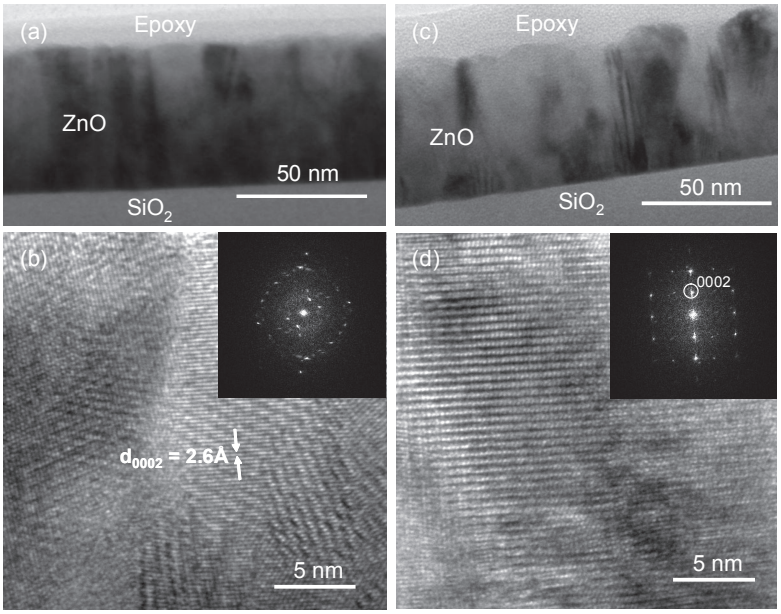


**Figure 5.** Low resolution (a and c) and high resolution (b and d) TEM images of the ZnO films grown at 250 (a and b) and 400 °C (c and d). Insets show digital diffractograms from the corresponding high resolution TEM images.

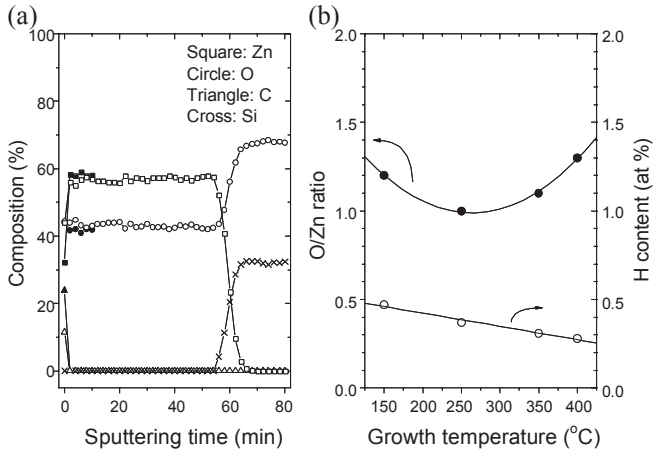


**Figure 6.** XPS depth profiles (a) of a ZnO film (open symbols) grown on $SiO_2$/Si at 250 °C and a single crystal (solid symbols). (b) O/Zn ratio and H content as a function of growth temperature.

tion of the carrier mobility by a factor of about 2 compared to the value in the *ab* plane.[27] Because the <002> preferred orientation of ZnO films is attenuated at lower growth temperatures, the mobility of the ZnO films with random orientation should decrease as the growth temperature decreases. The nearly-constant mobility at the growth temperature of 150 ~ 250 °C may be originated from a compromise between impurity scattering and piezoelectric scattering.

Figure 6a shows XPS depth profiles of the film (open circles) grown at 250 °C and ZnO single crystal (solid circles). Zn and O in the film are uniformly distributed from the surface to the interface between the film and substrate. The residual carbon content in the film is lower than the XPS detection limit (see the Supplementary Materials for the profiles of other films).

According to the depth profile by XPS, the O/Zn ratio of the film grown at 250 °C is evaluated be 0.77 which is much smaller than one expected from the stoichiometry of ZnO. It seems to be highly oxygen deficient in the film, but it is not true since the matrix effect of ZnO on the sputtering for depth profiling was not considered. Indeed, the O/Zn ratio (0.72) of single crystal is rather smaller than that (0.77) of the film. The low O/Zn ratio by XPS is originated from a preferential sputtering of oxygen to zinc during sputtering.[28] Therefore, the O/Zn ratio was non-destructively analyzed by RBS as shown in Figure 6b (solid circles). The O/Zn ratio of the ZnO film grown at 250 °C is ~ 1, but the ratio is rather larger than one in the films grown at higher and lower temperatures. Eventually, the ZnO films by ALD are not oxygen-deficient at least.

In the oxygen rich compositions, it is expected that oxygen interstitials ($O_I$) and zinc vacancies ($V_{Zn}$) may play a role of accepter-like defects resulting in *p*-type conductivity. However, the mobility and carrier concentration in Figure 3 reveal the *n*-type nature of the ZnO films grown by ALD, despite their zinc deficiency from the stoichiometry. It was reported through theoretical calculations that ZnO can not be doped *p*-type *via* native defects ($O_I$ and $V_{Zn}$), since the donor-like defects ($Zn_I$ and $V_O$) that could compensate *p*-type doping have low formation enthalpies at both Zn-rich and O-rich conditions.[29] Recently, Tan, *et al*. reported the change of conduction type from *n* to *p* occurred at an O/Zn ratio of 5 which is highly oxygen-rich.[30]

Figure 6b (open circles) shows the H contents in the films grown at 150 ~ 400 °C, analyzed by ERD. The H content decreases as the growth temperature increases. This is an opposite tendency to the increasing conductivity and carrier concentration as shown in Figure 2b and 3, respectively. In addition the H content is lower than 0.5 at % in the whole temperature range. This value corresponds to the hydrogen doping level of ~ $2 \times 10^{18}$/cm$^3$ which is much smaller than the measured carrier concentration in Figure 3. Therefore the incorporated hydrogen may only partially contribute to the *n*-type conductivity of ZnO films.

Figure 7a shows Zn $2p_{3/2}$ core level spectra of ZnO films and a single crystal. The binding energy of Zn $2p_{3/2}$ peak of the ZnO single crystal is 1021.4 eV, and those of the ZnO films are located in the range of 1021.6 ~ 1021.8 eV, shifting to higher binding energies at higher growth temperatures. However, it is quite difficult to distinguish the oxidation state of Zn in the films with Zn $2p_{3/2}$ peaks, since the $2p_{3/2}$ binding energy range (1020.8 ~ 1022.1 eV) of $Zn^0$ overlaps with that (1021.2 ~ 1022.5 eV) of $Zn^{2+}$ in ZnO.[31] On the other hand, the Zn LMM

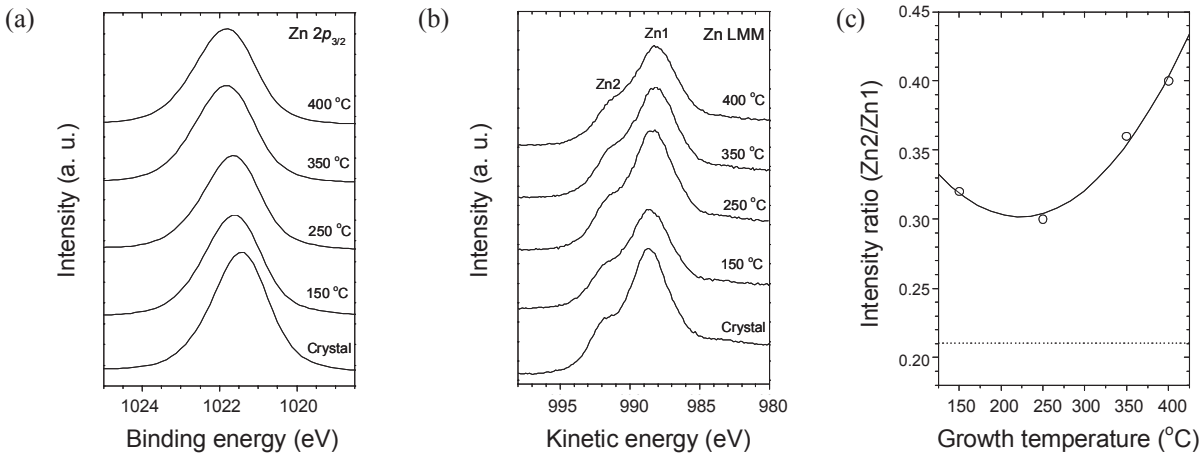


**Figure 7.** Zn $2p_{3/2}$ (a) and Zn LMM (b) core level spectra of the ZnO films grown at different temperatures and ZnO single crystal. The spectra were obtained after sputtering with $Ar^+$ of 0.5 keV for 4 min to remove the contaminant on the surface. (c) Zn2/Zn1 ratio as a function of growth temperature.

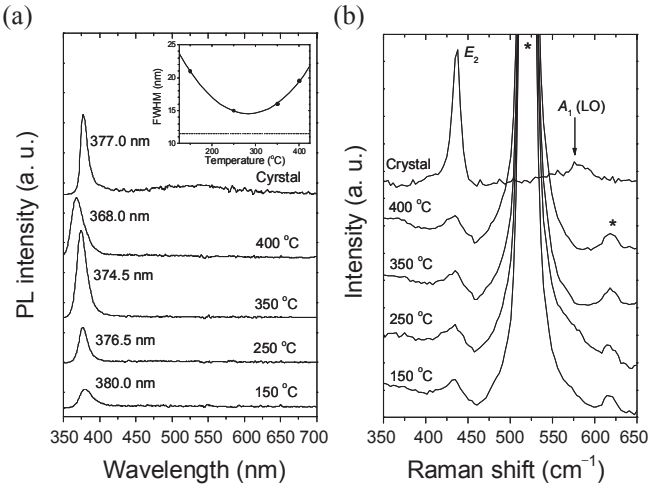


**Figure 8.** Room temperature PL (a) and Raman (b) spectra of ZnO single crystal and ZnO films grown at different temperatures excited with 325 nm. The inset in Figure 8a shows FWHM of the near band edge emission as a function of growth temperature. The asterisks in Figure 8b indicate the substrate peaks.

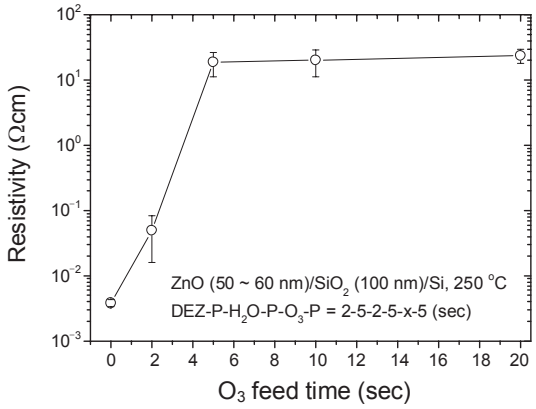


**Figure 9.** Resistivity of ZnO films as a function of ozone feeding time. The films were grown by the modified ALD sequence described in the Figure.

Auger spectra are more sensitive to differences in chemical environment than the Zn 2*p* spectra. The kinetic energy for the LMM peak of $Zn^0$ is ranged in 991.8 ~ 992.5 eV, and the LMM peak of $Zn^{2+}$ is located in the range of 987.7 ~ 988.9 eV.[31] Figure 7b shows the Zn LMM spectra of ZnO thin films and a single crystal. The lower kinetic energy peaks (Zn1: ~ 988.5 eV) are attributed to the bonding of Zn with oxygen in ZnO, whereas the shoulder peaks (Zn2: ~ 991.7 eV) indicate the presence of metallic zinc originated from $Zn_I$ and/or $V_O$. The metallic Zn to the oxidized Zn peak ratio (Zn2/Zn1) is plotted as a function of growth temperature in Figure 7c. The Zn2/Zn1 ratios in the ZnO films are much higher than ~ 0.21 in the single crystal as denoted with a dotted line. This reveals that the $Zn_I$ and/or $V_O$ are more incorporated in the films than in the single crystal. It should be noted that the Zn2/Zn1 varies with the growth temperature in a similar manner shown by the O/Zn ratio in Figure 6b. Although it is expected that the metallic zinc may be less incorporated in oxygen-richer ZnO films, the Zn2/Zn1 ratio of the films increases with the increasing O/Zn ratio. It may be due to the low formation energies of $Zn_I$ and/or $V_O$ even in the oxygen-rich condition.[29]

Figure 8a shows PL spectra of the ZnO films and the ZnO single crystal. For the single crystal, the strong emission from the band edge is observed at 377 nm due to the free-exciton recombination. For the ZnO films, the near band edge emission peaks are located at 368.0 ~ 380.0 nm shifting to lower wavelengths at higher growth temperatures. The inset in Figure 8a shows the full width at half maximum (FWHM) of the near band emission peaks as a function of the growth temperature. The FWHM of the film grown at 250 °C approaches to that (11.5 nm) of ZnO single crystal which was indicated with a dotted line in the inset.

The ZnO single crystal also shows weak and broad emission in green region. However the green emission is not observed from the ZnO films. It should be noted that the green emission is originated from oxygen vacancies.[32-34] It is recently reported that the ZnO film grown by ALD nearly does not have oxygen vacancies and does not emit light in the visible region.[35]

ZnO has a wurtzite structure with $C_{6V}$ point group symmetry. There are six Raman active modes: two $E_2$ vibrations at 101 and 437 cm$^{-1}$; one transverse $A_1$ at 381 cm$^{-1}$ and one transverse $E_1$ at 407 cm$^{-1}$; one longitudinal $A_1$ at 574 cm$^{-1}$ and one longitudinal $E_1$ at 583 cm$^{-1}$.[36] If the incident light is exactly normal to the surface of ZnO, only longitudinal $A_1$ and $E_2$ modes are observed, and the other modes are forbidden according to the Raman selection rules.[37] Figure 8b shows Raman spectra of the ZnO films and single crystal. In the ZnO single crystal, strong $E_2$ and broad longitudinal $A_1$ modes are located at 438 and 576 cm$^{-1}$, respectively. The wurtzite phase of ZnO films can be easily characterized particularly with the appearance of the high frequency $E_2$ mode at 435 cm$^{-1}$, although the longitudinal $A_1$ mode peak were not clearly resolved from the Si peak at 520 cm$^{-1}$. The absence of the $E_1$ mode at 583 cm$^{-1}$, which is associated with oxygen vacancy, also supports that the grown ZnO films barely have oxygen vacancies.[38]

To investigate the effect of oxidant on the conductivity of ALD ZnO films, ALD sequence was modified with ozone which is a stronger oxidant than water. Ozone exposure and purging steps were inserted between purging water and supplying DEZ. Therefore the modified ALD sequence is DEZ (2 s) – purging (5 s) – water (2 s) – purging (5 s) – ozone – purging (5 s) where the exposure time of ozone is varied from 0 to 20 s. ZnO films (50 ~ 60 nm) were deposited at 250 °C on $SiO_2$ (100 nm)/Si substrates with different feeding times of ozone by the modified sequence. The ozone concentration was 150 g/m$^3$ and the oxygen flow for the ozone generation was 800 sccm. Figure 9 shows that the resistivity of the ZnO films by the modified sequence rapidly increases from $3.8 \times 10^{-3}$ to 19.0 Ωcm as the ozone feeding time increases from 0 to 5 sec. However the resistivity is saturated at longer exposure times of ozone than 5 s. This reveals that the metallic zinc observed in the Zn LMM spectra may be additionally oxidized by ozone.

## Conclusion

ZnO films were grown by ALD using DEZ and water as a

Zn precursor and an oxidant, respectively. Resistivity of the films is in the order of $10^{-3}$ Ωcm showing a decreasing tendency at higher growth temperatures. In order to understand the high conductivity of ALD ZnO films, the films were characterized by XRD, TEM, XPS, ERD, RBS, PL, and Raman spectroscopy. In addition, the various analytical data of the ZnO films were compared with those of ZnO single crystal. According to our analytical investigation, metallic zinc in the films plays a role for the high conductivity of ALD ZnO. Therefore, the conductivity of ALD ZnO could be decreased by using a modified ALD sequence with additional oxidation step by ozone. This fundamental characterization of ALD ZnO films may facilitate conductivity modulation and *p*-type doping of ZnO for various device applications.

**Acknowledgments.** This work was supported by Konkuk University in 2008.

**Supplementary Materials.** SEM and AFM images and XPS depth profiles for ZnO films grown at different temperatures are available.

## References

1. Ozgur, U.; Alivov, Y. I.; Teke, L. A.; Reshchikov, M. A.; Dogan, S.; Avrutin, V.; Cho, S. J.; Morkoc, H. *J. Appl. Phys.* **2005**, *98*, 041301.
2. Hirschwald, W. H. *Acc. Chem. Res.* **1985**, *18*, 228.
3. Ellmer, K. *J. Phys. D: Appl. Phys.* **2001**, *34*, 3097.
4. Pearton, S. J.; Norton, D. P.; Ip, K.; Heo, Y. W. *J. Vac. Sci. Technol. B* **2004**, *22*, 932.
5. Wang, Z. L. *Materials Today* **2004**, *6*, 26.
6. Studenikin, S. A.; Golego, N.; Cocivera, M. *J. Appl. Phys.* **1998**, *84*, 2287.
7. Zhang, Y.; Zhang, Z.; Lin, B.; Fu, Z.; Xu, J. *J. Phys. Chem. B* **2005**, *109*, 19200.
8. Carcia, P. F.; McLean, R. S.; Reilly, M. H.; Nunes, G., Jr. *Appl. Phys. Lett.* **2003**, *82*, 1117.
9. Ortega-Lopez, M.; Avila-Garcia, A.; Albor-Aguilera, M. L.; Sanchez Resendiz, V. M. *Mater. Res. Bull.* **2003**, *38*, 1241.
10. Zhang, Y.; Du, G.; Yang, X.; Zhao, B.; Ma, Y.; Yang, T.; Ong, H. C.; Liu, D.; Yang, S. *Semicond. Sci. Technol.* **2004**, *19*, 755.
11. Lujala, V.; Skarp, J.; Tammenmaa, M.; Suntola, T. *Appl. Surf. Sci.* **1994**, *82/83*, 34.
12. Yamada, A.; Sang, B.; Konagai, M. *Appl. Surf. Sci.* **1997**, *112*, 216.
13. Kaiya, K.; Yoshii, N.; Omichi, K.; Takahashi, N.; Nakamura, T.; Okamoto, S.; Yamamoto, H. *Chem. Mater.* **2001**, *13*, 1952.
14. Park, S. H.; Lee, Y. E. *J. Mater. Sci.* **2004**, *39*, 2195.
15. Kim, S. K.; Hwang, C. S.; Park, S. H.; Yun, S. J. *Thin Solid Films* **2005**, *478*, 103.
16. Lee, S.; Im, Y. H.; Kim, S. H.; Hahn, Y. B. *Supperlattice Microst.* **2006**, *39*, 24.
17. Suntola, T. In *Handbook of Crystal Growth*; Hurle, D. T. J., Ed.; Elsevier: Amsterdam, 1994; Chapt. 3, p 601.
18. Maeda, K.; Sato, M.; Niikura, I.; Fukuda, T. *Semicond. Sci. Technol.* **2005**, *20*, S49.
19. Kohiki, S.; Nishitani, M.; Wada, T.; Hirao, T. *Appl. Phys. Lett.* **1994**, *64*, 2876.
20. Heiland, G.; Mollwo, E.; Stockmann, F. In *Solid State Physics*; Seitz, F., Turnbull, D., Eds.; Academic: New York, 1959; Vol. 8, p 191.
21. Van de Walle, C. G. *Phys. Rev. Lett.* **2000**, *85*, 1012.
22. Look, D. C.; Hemsky, J. W.; Sizelove, J. R. *Phys. Rev. Lett.* **1999**, *82*, 2552.
23. Janotti, A.; Van de Walle, C. G. *Appl. Phys. Lett.* **2005**, *87*, 122102.
24. Chen, L. Y.; Chen, W. H.; Wang, J. J.; Hong, F. C. N.; Su, Y. K. *Appl. Phys. Lett.* **2004**, *85*, 5628.
25. *CRC Handbook of Chemistry and Physics*; CRC Press: Boca Raton, FL, 2005.
26. Birkholz, M.; Selle, B.; Fenske, F.; Fuhs, W. *Phys. Rev. B* **2003**, *68*, 205414.
27. Littbarski, R. In *Zinc Oxide*; Hirschwald, W., Ed.; North-Holland: Amsterdam, 1981; Vol. 7, p 212.
28. Lee, J. M.; Kim, K. K.; Park, S.-J.; Choi, W.-K. *Appl. Phys. Lett.* **2001**, *78*, 3842.
29. Zhang, S. B.; Wei, S.-H.; Zunger, A. *Phys. Rev. B* **2001**, *63*, 75205.
30. Tan, S. T.; Chen, B. J.; Sun, X. W.; Yu, M. B.; Zhang, X. H.; Chua, S. J. *J. Electron. Mater.* **2005**, *34*, 1172.
31. Wagner, C. D.; Naumkin, A. V.; Kraut-Vass, A.; Allison, J. W.; Powell, C. J.; Rumble, J. R., Jr. *NIST X-ray Photoelectron Spectroscopy Database*, available in http://srdata.nist.gov/xps/.
32. Vanheusden, K.; Warren, W. L.; Seager, C. H.; Tallant, D. R.; Voigt, J. A.; Gnade, B. E. *J. Appl. Phys.* **1996**, *79*, 7983.
33. Vanheusden, K.; Seager, C. H.; Warren, W. L.; Tallant, D. R.; Voigt, J. A. *Appl. Phys. Lett.* **1996**, *68*, 403.
34. Leiter, F. H.; Alves, H. R.; Hofstaetter, A.; Hofmann, D. M.; Meyer, B. K. *Phys. Stat. Sol. B* **2001**, *226*, R4.
35. Lim, J.; Shin, K.; Kim, H. W.; Lee, C. *J. Lumin.* **2004**, *109*, 181.
36. Damen, T. C.; Proto, S. P. S.; Tell, B. *Phys. Rev.* **1966**, *142*, 570.
37. Zhaochun, Z.; Baibiao, H.; Yongqin, Y.; Deliang, C. *Mater. Sci. Engin. B* **2001**, *86*, 109.
38. Cui, J. B.; Daghlian, C. P.; Gibson, U. J.; Pusche, R.; Geithner, P.; Ley, L. *J. Appl. Phys.* **2005**, *97*, 044315.